Noname manuscript No.
(will be inserted by the editor)

Robust DOA Estimation and Target Docking for Mobile Robots

Received: date / Accepted: date

Abstract Direction of arrival (DOA) guided automated target acquisition and docking system is proposed for mobile robots employing the dual-directional antenna system. The dual-directional antenna estimates the DOA of the signal of interest using the ratio of the signal strengths between two adjacent antennas. In practice, DOA estimation poses a significant technical challenge, since the RF signal is easily distorted by the environmental conditions. Therefore, the robot often loses its way in an electromagnetically disturbed environment. To cope with this problem, a robust DOA estimation algorithm is developed based on Kalman filtering. This algorithm allows the robot to reduce the potential error in the estimated DOA, and adjust the robot's heading to the target transponder without needing to know the positions of current and previous measurements in a global coordinate system. The simulation and experiment results clearly demonstrate that the mobile robot equipped with the developed system is able to dock to a target transponder in an indoor environment partially occupied by obstacles.

Keywords RFID · DOA · dual-directional antenna · Kalman filtering · docking

1 Introduction

When robots are deployed into a real environment to perform their mission, they need to accurately and efficiently identify the environment and move toward a specific target. Numerous attempts have been made to solve this fundamental issues of identification and localization [18]. Among them, vision has been a well-tried method, but its accuracy is affected by the environmental conditions such as changes in illumination, occlusion, and line

of sight problems [19,20]. Recent advances in sensor and networking technologies provide new approaches aimed at structuring an easy to understand environment with networked embedded devices such as wireless sensors and RFID transponders [8,21]. Such an environment allows the robot to retrieve complex information about a specific object most easily, but does not usually support localization unless a GPS receiver is included in sensors. The problem of localization thus remains a significant technical challenge in this approach.

Location estimation can be divided as range-based and bearing-based approaches. The range-based approaches trilaterate the transponder position using the estimated distances from the reference points. The distance can be estimated from received signal strength (RSS) measurements [10–12] or time difference of arrival (TDOA) scheme [9,22]. RSS-based schemes are easily implementable, but the accuracy is highly dependent on the environment and the distance. In contrast, TDOA based approaches using RF and ultrasonic signals offer fairly high accuracy, but the ultrasonic signals are subject to multi-path propagation effects and the optical line of sight. To be more specific, a major difficulty with range-based schemes for mobile robot applications lies in the uncertainty of the robot heading. The robot needs to keep track of its orientation to a target. On the other hand, bearing-based schemes use the direction of arrival (DOA) of a target signal using, for instance, arrays of multiple ultrasonic sensors [13,14]. They have received more attention recently and considered to be better suited for the mobile robot applications.

Therefore, in this work, we attempt to develop a new bearing-based *ad hoc* target acquisition and docking system using RFID technology for mobile robot applications. Bearing information can be achieved in RFID by replacing the omni-directional antenna, generally used in the active RFID readers, with the directional antenna. Specifically, a dual-directional antenna was designed to estimate the DOA in real time and cover as large an area as possible at a time, which was demonstrated in the authors' earlier works [15,16]. We paid attention to the capability of an off-the-shelf mobile robot equipped with the dual-directional antenna that could estimate the DOA of the signal of interest from the ratio of the RSS measurement between two adjacent antennas. However, the RSS ratio of the dual-directional antenna will oscillate by the effect of neighboring obstacles in a cluttered environment. This motivated us to apply the Kalman filter based technique to the ratio data, helping the robot find the direction of the signal more accurately under such conditions. We demonstrate that the robot can navigate to a target by adjusting its heading according to the filtered ratio without needing to know the positions of current and previous measurements in a global coordinate system.

This paper is organized as follows. In Section II, the developed RFID system is explained with the fundamentals of electromagnetic theory underlying the measurement of the DOA. In Section III, the problem of the DOA estimation affected by the multi-path propagation is addressed and analyzed. Section IV describes the proposed ratio filtering and robot navigation algorithm. Simulation and experiment results are shown in Section V. Finally, conclusions are drawn in Section VI.

2 DOA Estimation Using a Dual-directional Antenna

Our approach is based on the estimation of the DOA of signal sources. For the purpose, a dual-directional antenna was developed that replaces omni-directional antennas generally used in active RFID systems. The dual-directional antenna was designed in such a way that two adjacent identical loop antennas are positioned perpendicularly to each other as shown in Fig. 1. An efficient implementation of DOA estimation of RF signals is based on classical electromagnetic theory detailed and explained below.

When an electromagnetic signal is transmitted to the dual-directional antenna mounted on top a mobile robot as illustrated in Fig. 1, voltages are induced from each antenna in proportion to the absolute of the magnetic flux that passes through each antenna as

$$V_1 \propto |CSBsin(\theta - \varphi)/r| \tag{1a}$$
$$V_2 \propto |CSBsin(\theta - \varphi + 90^\circ)/r|\,, \tag{1b}$$

where S is the surface area of the antenna, B is the magnetic flux density of the wave passing through the antenna, θ is the antenna rotation (or facing) angle with respect to the robot's heading, φ is the DOA of the received signal, C accounts for the environmental conditions, and r is the traveling distance of the signal from the transponder, respectively. Assuming that r will exceed a one quarter wavelength, the voltage will be inversely proportional to r [1–4]. Note that the antenna can rotate independently of the robot. In this work, the angles are positive if they are measured in the counterclockwise direction.

Since the antennas are perpendicularly positioned to each other, the induced voltage has a phase difference of 90°. Now a dimensionless parameter can be defined as the ratio of the magnitudes of the induced voltages or signal strengths given by

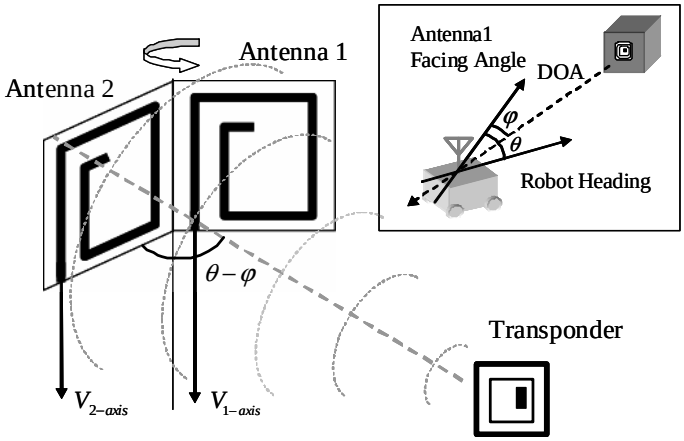

Fig. 1 Azimuth angle of the direction of arrival of a signal

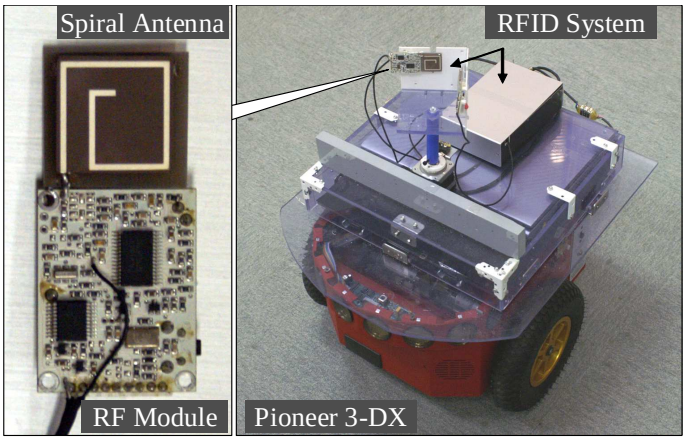

Fig. 2 Mobile robot equipped with DOA sensing RFID system

$$\nu_{12} = V_1/V_2 = |tan(\theta - \varphi)|. \tag{2}$$

Then, the DOA of the received signal can be determined from Eq. 2.

Fig. 2 shows the developed DOA guided target acquisition and docking system employing the proposed dual-directional antenna. The system is composed of the following two parts: 1) an RFID reader interacting with RFID transponders, and 2) a Pioneer 3-DX mobile robot onto which the reader is installed. The RF modules and antennas, manufactured by Ymatics LTD. [24], operate on 303.2 MHz frequency using a 3 V supply. The reader contains a microprocessor ATmega2560 and a set of two RF modules. The modules read identifiers and the strength of the signal of interest received from highly directional spiral loop antennas and transmit them to the microprocessor through a standard RS-232 interface. The antennas are perpendicularly positioned on the antenna base that is mounted on a stepping motor. The microprocessor estimates the DOA from the changes in the received signal strength according to the antenna facing angle controlled by the stepping motor.

Fig. 3 shows the RSS and the ratio curves according to the antenna angle measured using the developed system. The left graph shows the RSS and the right graph is the ratio curve. Under non-ideal measurement conditions, the erroneous offset voltage caused by the white noise and the system conditions will probably be included in the RSS as shown in the figure. The maximum and minimum level of the ratio therefore will change according to the actual working condition of the system. This makes it difficult to precisely estimate the DOA directly from the ratio. However, even though the ratio changes by the variation of the offset level, there always exists a stationary point on the ratio curve. When a transponder is located on the center line between both antennas, the ratio is 1.0 regardless of the offset voltage. And the ratio increases and decreases as the transponder moves left or right, respectively. Therefore, the robot can know the change of the direction then find the

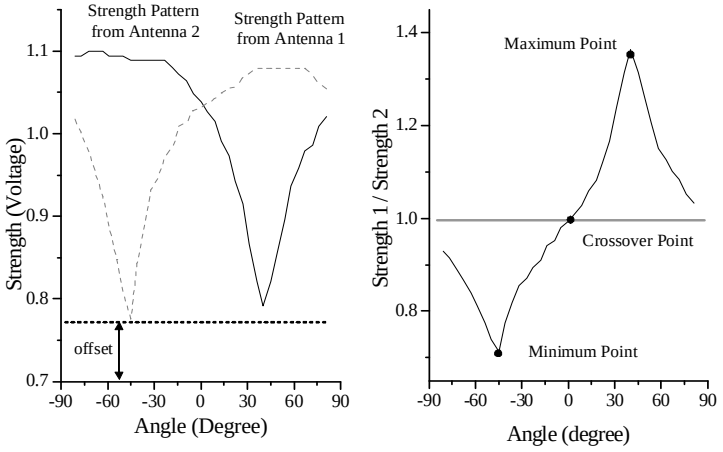

Fig. 3 RSS and ratio curves measured using the dual-directional antenna

direction to a transponder by adjusting its heading toward the direction in which the ratio approaches 1.0.

3 RF Signal Distortion by Multi-path Propagation

This section will give some insight into how the RSS ratio changes in a real environment. Fig. 4 shows the changes in the RSS ratio when the transponder moves in our hallway condition. Two environmental conditions are tested with no obstacles and a single obstacle, respectively. When the transponder

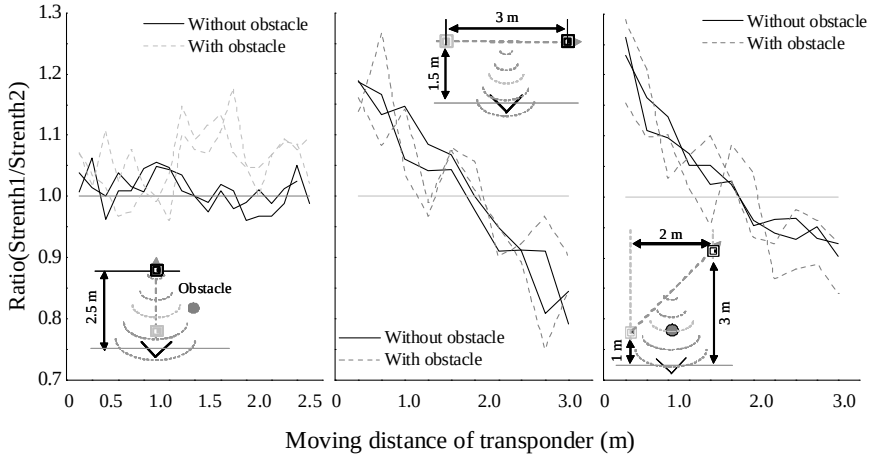

Fig. 4 RSS ratio changes while transponder moves (left) vertically, (center) horizontally, (right) diagonally

moves vertically, the bearing of the transponder will remain unchanged, so does the ratio. In contrast, the ratio will decrease or increase as the bearing of the transponder changes when the transponder moves horizontally or diagonally. In the figure, the ratio does not show a clear pattern linearly changing with the transponder bearing, and tends to oscillate. It is also evident that the distortion of the curve increases when the RF signal is affected by a nearby obstacle. Note that our environment was not electromagnetically shielded, thus the transmitted signal was distorted by the multi-path propagation effects even though there was no obstacles [5,6,17]. Based on the above results, we will only be able to approximately estimate the DOA of the signal from the ratio. This potentially is a big problem in direction finding under real-world environment conditions.

Fig. 5 briefly shows the multi-path propagation of RF signals due to the presence of the obstacles that reflect, refract, and scatter the propagating signals. The antenna, therefore, will receive a large number of waves with various amplitudes, phases, and directions. Thus, a total of magnetic flux, denoted hereafter by Φ, will be the sum of the magnetic flux of the direct wave from the transponder and that of the diffracted, non-direct waves represented by

$$\Phi_{tot} = \Phi_{direct} + \sum_{i=1}^{n} \Phi^{i}_{non-direct}. \tag{3}$$

Note that, the magnetic flux can be expressed as (see Eq. 1)

$$\Phi = \frac{CSRB}{r} \sin(\theta - \varphi), \tag{4}$$

where R is the coefficient of the strength of the arrival signal (*e.g.*, $R = 1$ when the wave is the non-diffracted, direct wave). Assuming that the direct

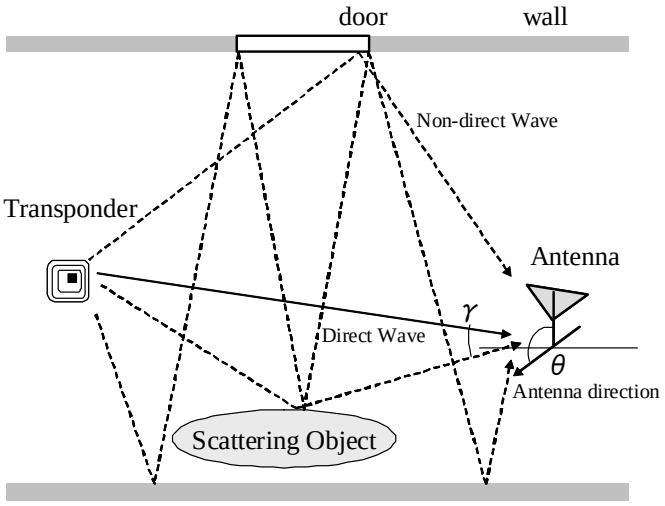

Fig. 5 Multi-path propagation in real environment

and non-direct waves have the differences in the angle of incidence, γ_i, and the traveling distance, Δr_i, respectively, Eq. 3 can be expanded as

$$\Phi_{tot}=\frac{CSB_0}{r_0}\sin(\theta-\varphi_0)+\frac{CSR_1B_1}{r_0+\Delta r_1}\sin(\theta-\varphi_0+\gamma_1)+\ldots. \tag{5}$$

Here, the magnetic flux density B_i of the signals have phase differences according to the ratio between the traveling wave distance difference Δr_i and the wave length λ given by $2\pi\Delta r_i/\lambda$. The phase difference yields the changes in the amplitude of the received signal. If we denote the term $\frac{CSR_iB_i}{r_0+\Delta r_i}$ as a_i and $(\theta-\varphi_0)$ as χ, Eq. 5 can be rewritten as

$$\Phi_{tot}=a_0\sin(\chi)+a_1\sin(\chi+\gamma_1)+\ldots\quad. \tag{6}$$

After some mathematical manipulation, we can get the following equation.

$$\Phi_{tot}=A\sin(\chi+\eta), \tag{7}$$

where

$$A=\left[\left(a_0+\sum_{i=1}^{n}a_i\cos(\gamma_i)\right)^2+\left(\sum_{i=1}^{n}a_i\sin(\gamma_i)\right)^2\right]^{1/2}, \tag{8a}$$

$$\eta=\tan^{-1}\left\{\frac{\sum_{i=0}^{n}a_i\sin(\gamma_i)}{a_0+\sum_{i=1}^{n}a_i\cos(\gamma_i)}\right\}. \tag{8b}$$

Note that A and η are obtained by combining a variety of a_i and γ_i. Therefore, it is almost impossible to find the exact direction of the transponder directly from the ratio pattern. This makes it difficult for a robot to find its way to the transponder position in the cluttered environment. The worst case estimates of the DOA will occur when the denominator of the arctangent function argument becomes zero in Eq. (8b). In this case, the estimation error η will increase or decreases to $\pm90°$. However, the non-direct wave travels a longer distance than the direct wave and its strength is reduced by the obstruction. Thus, the magnitude of the non-direct wave is much smaller than that of the direct wave, and the denominator does not virtually become zero in most cases. Therefore, a limited number of non-direct waves will affect the DOA estimation. To the best of our knowledge based on the above-described investigation, we can confidently say that the error will always be less than $\pm90°$. Moreover, if a large magnitude of errors can be filtered and fall into a reasonable range, then the robot can move close to the transponder. The following section will discuss a simple, yet effective way of filtering DOA estimation errors.

4 Robust DOA estimation and Navigation Algorithm

In this work, the robot is commanded to move and dock to the target transponder by simply following the DOA of the transponder signal without the need for any additional sensor. However, as shown in Fig. 4, the

RSS ratio under real-world conditions that contain obstacles shows irregular fluctuations from which the robot needs to estimate the DOA of the target signal. It is thus often the case that the robot's path will be deflected in unexpected ways, making the robot move in a zigzag manner and sometimes lose its target with a large amount of DOA estimation error. To enable the robot to move reliably and efficiently toward the target position, it is required to minimize the estimation errors and to smooth the fluctuations in the ratio. To cope with this problem, the Kalman filtering based technique is applied to an entire data set of the ratio.

Note that, it is almost impossible to quantify the error from the RSS ratio, but there seems to be a tendency for this ratio to change in a regular pattern as the robot (or the transponder) moves uniformly. If the robot (or the transponder) moves with a constant velocity as shown in Fig. 4, the distance Δr_i and the bearing γ_i also change in a linear fashion. Then the ratio oscillates as shown in the figure, which can be conjectured from Eq. 5. The ratio will be directly affected by the differences in the angle of incidence, the phase, and the strength between the direct and non-direct waves. Since the wave length of 315 MHz signals is about 1 m, the changes in Δr_i may not significantly affect the ratio until the robot movement interval exceeds at least several tens of centimeters. Note here that any location-awareness system can allow coarse-grained location information to be provided to the robot. Then there can be practical reasons for designing an indoor mobile robot that is able to dock to transponders located within 5 to 10 m away. Under such circumstances, only a small number of data points will be available while the robot moves to the target transponder. Thus, we developed a filtering algorithm based on the simple and fundamental form of Kalman filter implementation [7].

Assuming that the ratio is measured at a uniform interval, the ratio at the current measurement step, ν_n, is the summation of the ratio at the previous measurement step, ν_{n-1}, and an unknown incremental amount of ratio, $\Delta\nu$, given by

$$\nu_n = \nu_{n-1} + \Delta\nu. \tag{9}$$

Since an unknown amount of error, η, is included in ν_n, especially in obstacle cluttered environments, ν_n can be corrected by multiplying $\Delta\nu$ by a gain factor, g_n, as

$$\nu_n^* = \nu_{n-1}^* + g_n \cdot \Delta\nu, \tag{10}$$

where ν_n^* and ν_{n-1}^* are the filtered ratios at the current and the previous measurement step, respectively. It is straightforward to express Eq. 10 as

$$\nu_n^* = \nu_{n-1}^* + g_n \cdot (\nu_n - \nu_{n-1}^*). \tag{11}$$

Here the gain is updated, reflecting the relation of the measured ratio at the current step and the filtered ratio at the previous step using the variance of their values as

$$g_n = VAR(\nu_{n-1}^*)/VAR(\nu_n). \tag{12}$$

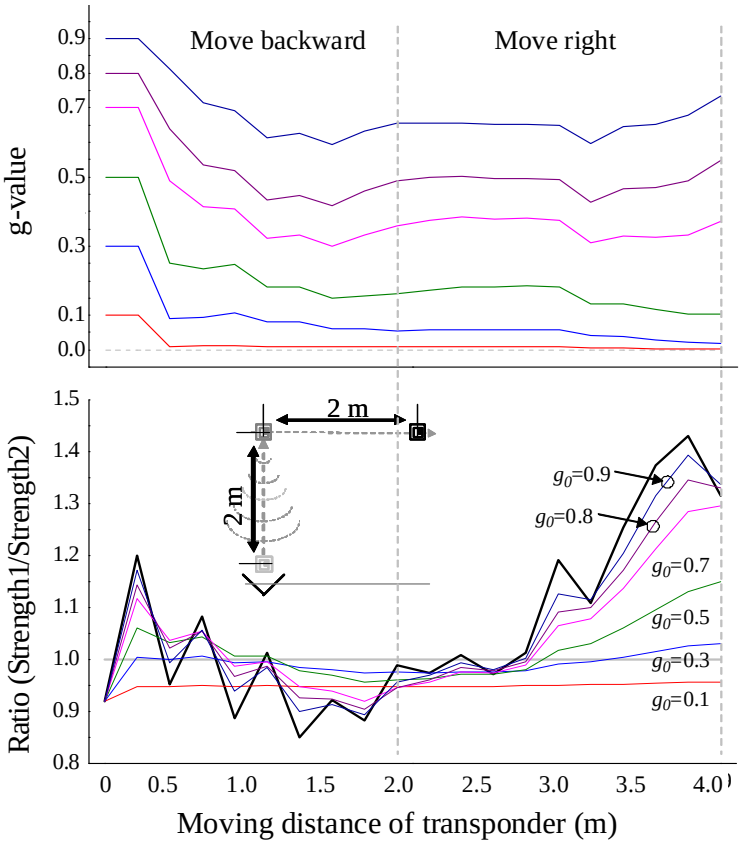

Fig. 6 (upper) Change in the value of the gain, (lower) the filtered ratio according to the initial value of the gain

Fig. 6 shows a typical example of how the filtered ratio changes according to the initial value of the gain. The ratio pattern was obtained when a transponder was moving 2 m backward, leaving the direction unchanged, and moving subsequently 2 m to the right in our hallway environment. The thick solid line in the lower graph shows the non-filtered data. The upper graph shows the changes in the gain when different values of initial gain g_0 were selected. If there are large fluctuations in the ratio, the variance increases. Then the gain decreases accordingly, allowing the filtered values to be smoothened. In contrast, if the gain increases with small fluctuations, the filtered values becomes closer to the measured values. As shown in the upper graph, when g_0 is less than 0.5, g_n converges to zero. However, if g_0 exceeds 0.5, the gains would increase or decrease in a similar fashion. If the number of measurement points are large enough, the gain becomes more suitable for each measurement point. However, up to several dozen measurement points in ordinary sized spaces, the proposed filtering depends heavily on the initial value g_0 assumed. The lower graph shows an example about the relation

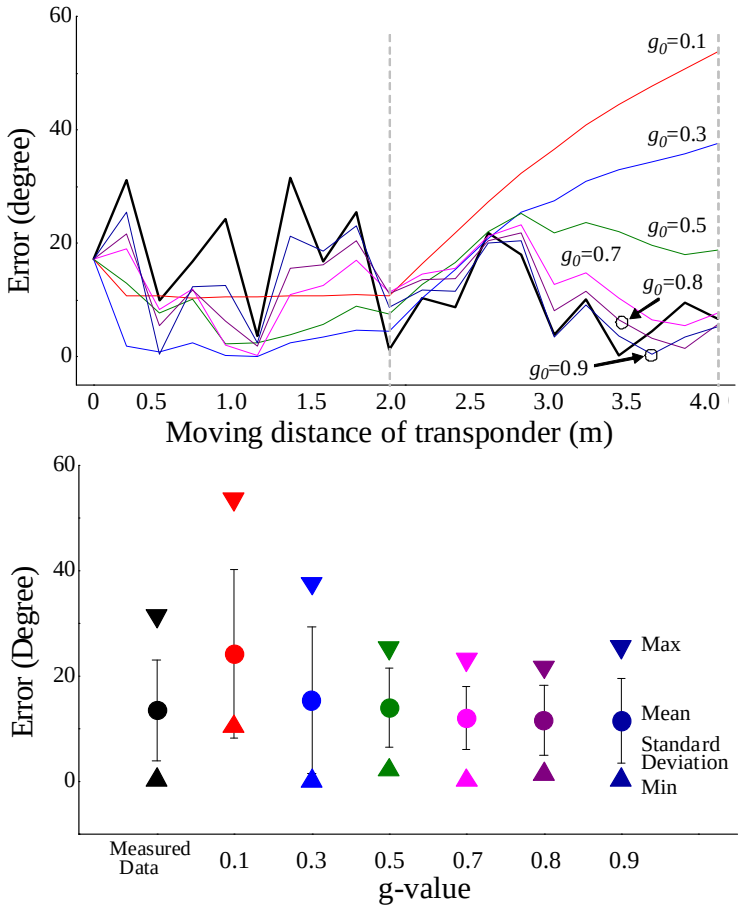

Fig. 7 (upper) Error in DOA estimation, (lower) error statistics according to the initial value of the gain

between g_0 and the filtered ratios. Note that the value of g_0 falls within the range between 0 and 1. If g_0 is small, the measurement flattens out. On the other hand, a large value of g_0 will cause the filtered ratio to more closely follow the measurement data. Fig. 7 shows how the filtering improves the direction finding accuracy. The mean and the standard deviation of the error across the forty measurement points are also shown in the lower graph. As shown in the figure, a low gain may worsen the accuracy of the measurement. We empirically evaluate the accuracy of each gain and select the initial value between 0.7 and 0.8.

Fig. 8 shows the filtered ratio when a neighboring obstacle is located similar to the case of Fig. 4. Even though the distortions in the measured ratio are significant by the effects of multi-path propagation, the proposed algorithm can effectively flattens out the large variations. Note that, the ratio level of 1.0 is the intersection point at which the signal strengths of Antenna

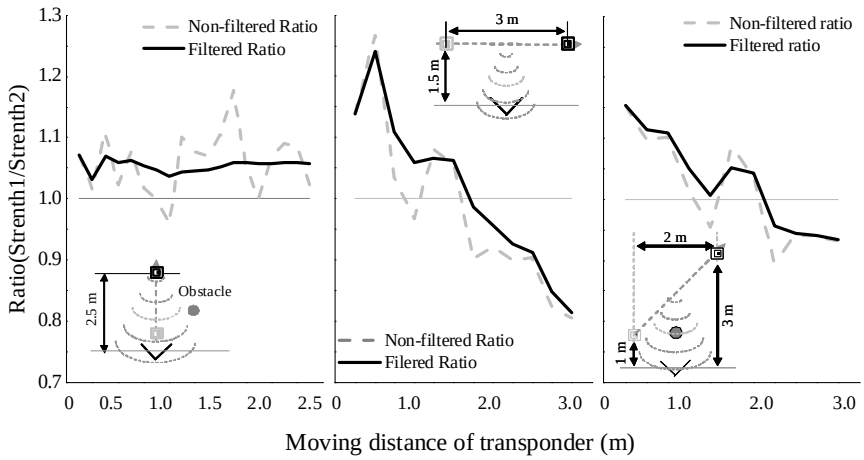

Fig. 8 Filtered and non-filtered RSS ratio while the transponder moves (left) vertically, (center) horizontally, (right) diagonally

♯1 and Antenna ♯2 meet when the transponder is located in front of the two antennas. The ratio increases or decreases as the DOA changes, and can not give an exact direction to the transponder. But, the key idea is that the expected position of the transponder can be located on the right or left side with respect to the center line giving the ratio level of 1.0.

Based on the principle of finding directions, the robot can navigate to the target transponder by adjusting its heading toward the ratio of 1.0. Thus, if we control the wheel velocities of the robot according to the ratio, the robot can follow the direction of the transponder. Fig. 9 shows the line that fits the ratio data with respect to θ, the bearing between the antenna and the DOA of the signal, given by

$$\nu* = \frac{1}{h}\Theta + 1.0, \tag{13}$$

where $\frac{1}{h}$ is the slope of the fitted line. Then the heading θ of the robot is determined as follows:

$$\theta = h(\nu* - 1.0), \tag{14}$$

whereby the rate of the rotation of the wheel can then be controlled accordingly.

5 Experiment Results of Robot Docking

5.1 Simulation Results

To verify the validity of the proposed DOA filtering and robot navigation algorithm, we performed experiments on autonomous target docking using the simulator developed in-house. Since it is almost impossible to include

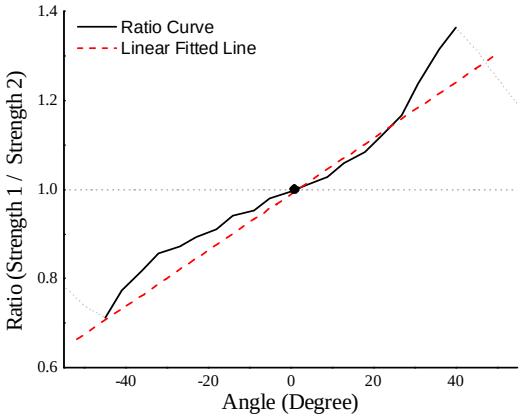

Fig. 9 Relationship between the ratio and the angle

the whole scattering effect of signals in the obstacle cluttered environment, we implemented the basic ray-tracing principle explained in Section 3. Fig. 10 shows the layout of the developed simulator. In Fig. 10, the environment panel shows the simulation environment including a robot, a transponder, and obstacles. The grid lines are drawn with segments of 50 $cm \times 50$ cm. The number and location of the object within the environment is modified by the upper control panel, and the DOA estimation and the robot navigation are controlled by the lower control panel. The ratio and directions are shown in the graph panel while the robot moves. Also, the robot moving path is shown in the environment panel.

The conditions assumed in the simulation are as follows.

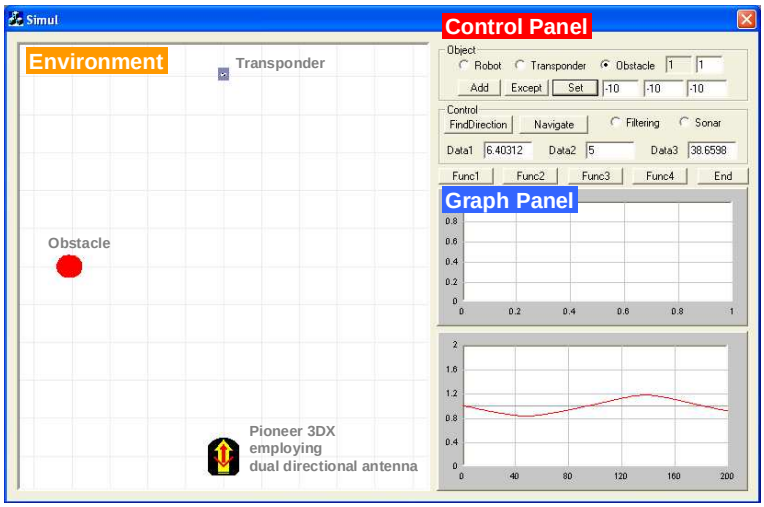

Fig. 10 Layout of the simulation environment

- The transponder is stationary and considered as a point charge.
- Obstacles scatter signals with fixed rate R of either 0.2, 0.5, or 0.7
- Intrinsic sensing error of $\pm 4^\circ$ with the Gaussian distribution is included in estimating the DOA.

The suggested sensing error range is based on the fact that have been obtained from the authors' earlier experiments in an obstacle-free environment [23]. Under the above conditions, the robot navigates according to the following steps.

1. The robot scans the transmitted signal from -90° to 90° and estimates the DOA of the signal by finding the intersection point of the ratio with the level of 1.0.
2. The robot moves to the estimated DOA and adjust its heading by controlling the rotational velocity of wheels according to the ratio.
3. If the distance measured from the signal strength becomes less than 50 cm, then the robot stops moving.

Simulations were conducted under various test conditions as shown in Fig. 11. In each condition, the left figure shows the case of the non-filtered ratio, and the right figure shows the case of the filtered ratio. The transponder was positioned at 4 m away from the robot. The dots show the path that the robot traced. Fig. 11-(a) shows the results in an empty space. Under this condition, there exists only an error of $\pm 4^\circ$ resulted from the intrinsic accuracy, thus the robot moves straight irrespective of whether the robot uses the proposed algorithm. Fig. 11-(b) shows the condition that an obstacle whose scattering rate is 0.5 is positioned between the transponder and the robot. Since the signal is distorted by the environmental effect, the robot navigates away from the obstacle. It is notable that the proposed filtering algorithm gives a smoother path. The accuracy and robustness of DOA estimates is largely dependent on environmental conditions. Thus more abrupt turns can be seen in robot paths under more cluttered environments. In Fig. 11-(c), where the robot navigates through randomly positioned obstacles with the same scattering rate of 0.5, the robot can not reach the transponder position without the proposed filtering algorithm. In Fig. 11-(d), obstacles have a different scattering rate of either 0.2, 0.5, or 0.7. Also, one obstacle displayed by the red square moves half the speed of the robot. The moving obstacle can cause an abrupt change in the received RF signal, particularly when it is moving toward the robot. However, the proposed algorithm gives an effective and reliable path to the transponder by flattening out and correct the large variation in the RSS ratio. This is because abrupt changes in the estimation direction could effectively be absorbed through the proposed filtering method.

Fig. 12 shows the estimated ratios and corresponding DOA errors as the robot moves toward the target transponder in the case of Fig. 11-(c). The left graphs show the ratios and the right graphs are the absolute values of the errors in the DOA estimates. Following the estimated ratio as shown in Fig. 12-(a) that fluctuates and oscillates, the robot can not find the correct direction. In contrast, by filtering the ratio as shown in Fig. 12-(b), the ratio

Table 1 Changes in the dock success rate using the filtering algorithm

No. of Obstacles	Without Algorithm			With Algorithm		
	Success	Fail	Rates(%)	Success	Fail	Rates(%)
0	50	0	100	50	0	100
1	49	1	98	50	0	100
7	39	11	78	44	6	88
7/1(moving)	35	15	70	43	7	86

is smoothened out and the error decreases, which helps the robot dock to the target position successfully.

Table 1 shows a statistical investigation of robot self-docking to the target using the same simulation environment. The target was positioned 4 m away from the robot in different environmental conditions. 50 trials were tested based on the non-filtered ratio, and the same number of trials were performed under the same conditions employing the proposed filtering algorithm. We randomly set the number and position of obstacles for each trial. Note that when signals interfered with by obstacles, the error increased. However, it is evident that the dock success rate was higher when the filtering algorithm was employed.

5.2 Experimental Results

To verify the validity of the proposed algorithm in a real environment, we performed experiments with the mobile robot system shown in Fig. 2 in our hallway environment. There were a metallic door and an elevator in the hallway. The target transponder is located at the position of (0, 3) m in a Cartesian coordinate system whose origin is at the initial position of the robot. The robot moves to the acquired target guided by the ratio estimated from the RFID system. The robot stops approaching the transponder, when the transponder is within the range of 30 cm from the robot. This distance is estimated from the signal strength and sonar sensors positioned around the robot.

The experimental results are shown in Fig. 13. The robot starting from the initial position marked with a black circle moves to the transponder marked with a gray circle. The robot path is displayed by dots connected by lines. The red dots are the path guided by the originally estimated ratio, and the blue square dots are made by the filtered ratio. Fig. 13-(a) shows the case that no neighboring obstacle is positioned in the environment. The robot could arrive at the transponder position in both cases. Note that the error in the estimated DOA is affected by the numbers, positions, and physical properties of the obstacles. Fig. 13-(b) shows the case that a large DOA estimation error occurs when the neighboring obstacles, four metallic chairs and one person, interfere with the signal transmission. The ratio was distorted too much, thus the robot could not arrive at the transponder position. However, when the ratio was filtered by proposed algorithm, the robot could arrive at the transponder position.

The simulation and experiment results show the proposed filtering algorithm is very useful to the robot docking in a cluttered environment. However, the robot still may not arrive at the target in many cases as shown in Table 1. The robot moves to the transponder by controlling the wheel velocities according to the ratio using Eq. 14. Here the gain h is set to a constant value determined from the ratio curve as shown in Fig. 9. However, the relationship between the ratio and the angle is not always obvious and changes by surrounding and system conditions. Therefore, we need to modulate the gain h depending on the changes in the ratio.

6 Conclusion

Autonomous mobile robot navigation and docking was demonstrated in an indoor environment guided by the ratio of received signal strengths from the dual-directional antenna. To cope with the effects of multi-path propagation, a simple, yet effective correction algorithm was proposed for uncertain DOA estimation. The proposed algorithm reduced potential errors in the estimation at every step based on Kalman filtering, which helped a robot not to lose the direction to the target. The simulation and experiment results verified that the robot could arrive at the target position even though the RF signal was significantly interfered with by the obstacles. Our major contributions can be summarized as: 1) the proposed algorithm gives the most feasible direction to facilitate the finding of the transponder when the robot suffers from an unknown amount of errors in DOA estimation. Therefore, 2) the proposed RFID reader improves the capability over the current state-of-the-art in RFID technology and can be applied to a variety of industrial applications. Our future effort includes the use of additional sensor data to be fused for enhancing the navigation capability of the robot in a more cluttered environment.

References

1. J. R. Reitz (1993) Fundations of Electromagnetic Theory, Addison Wesley
2. D. Halliday, R. Resnick, J. Walker (1997) Fundamentals of Physices, John Wiley & Sons, Inc.
3. W. L. Stutzman, G. A. Thiele (1999) Antenna Theory and Design, John Wiley & Sons Ltd.
4. C. A. Balantis (1996) Antenna Theory: Analysis and Design, Wiley Text Books
5. L. Tsang, J. A. Kong (2001) Scatterning of Electromagnetic Waves : Advanced Topics, John Wiley & Sons Ltd.
6. T. S. Rapaport (2002) Wireless Communications, Prentice-Hall, Inc.
7. E. Brookner (1998) Tracking and Kalman Filtering Made Easy, John and Willey & Sons, Inc.
8. N. Y. Chong, H. Hongu, K. Ohba, S. Hirai, K. Tanie (2004) A Distributed Knowledge Network for Real World Robot Applications, Proc. IEEE/RSJ Int. Conf. on Intelligent Robots and Systems 187-192
9. A. Smith, H. Balakrishnan, M. Goraczko, N. Priyantha (2004) Tracking Moving Devices with the Cricket Location System, Proc. 2nd Int. Conf. on Mobile Systems, Applications, and Services 190-202
10. J. Hightower, G. Borriello, R. Want (2000) SpotON : An Indoor 3D Location Sensing Technology Based on RF Signal Strength, UW CSE Technical Report

11. D. Niculescu, B. Nath (2001) Ad hoc positioning system (APS), Proc. IEEE Global Telecommnication Conf 2926-2931
12. P. Bahl, V. N. Padmanabhan (2000) RADAR: An In-Building RF-Based User Location and Tracking System, Proc. IEEE INFOCOM 2:775-784
13. N. Priyantha, A. Chakaborty, H. Balakrishnan (2000) The Cricket Location-support System, Proc. 6th ACM MOBICOM 32-43
14. D. Niculescu, B. Nath (2003) Ad hoc positioning system (APS) Using AOA, Proc. INFOCOM 1374-1742
15. M. Kim, N. Y. Chong (2006) Enhancing RFID Location Sensing Using a Dual Directional Antenna, Proc. 6th Asian Control Conference 964-970
16. M. Kim, H. W. Kim, N. Y. Chong (2007) Automated Robot Docking Using Direction Sensing RFID, Proc. IEEE Int. Conf. on Robotics and Automation 4588-4593
17. F. A. Alves, M. R. L. Albuquerque, S. G. Silva, A. G. d'Assuncao (2005) Efficient Ray-Tracing Method for Indoor Propagation Prediction, Proc. SBMO/IEEE MTT-S Int. Conf. on Microwave and Optoelectronics, 435-438
18. J. Hightower, G. Borriello (2001) Location Systems for Ubiquitous Computing, IEEE Computer Magazine, 34:57-66
19. D. C. K. Yuen and B. A. MacDonald (2005) Vision-Based Localization Algorithm Based on Landmark Matching, Triangulation, Reconstruction, and Comparison, IEEE Transactions on Robotics 217-226
20. S. Se, D. G. Lowe, J. J. Little (2005) Vision Based Global Localization and Mapping for Mobile Robots, IEEE Transactions on Robotics 364-375
21. L. E. Holmquist, H. W. Gellersen, G. Kortuem, S. Antifakos, F. Michahelles, B. Schiele, M. Beigl, R. Maze (2004) Building Intelligent Environments with Smart-Its, IEEE Computer Graphics and Applications 24:56-64
22. L. M. Ni, Y. Liu, Y. C. Lau, A. P. Patil (2004) LANDMARC : Indoor Location Sensing Using Active RFID, ACM Wireless Networks 10:701-710
23. M. Kim, N. Y. Chong (2007) RFID-based Mobile Robot Guidance to a Stationary Target, Mechatronics 17:217-229
24. www.ymatics.co.jp

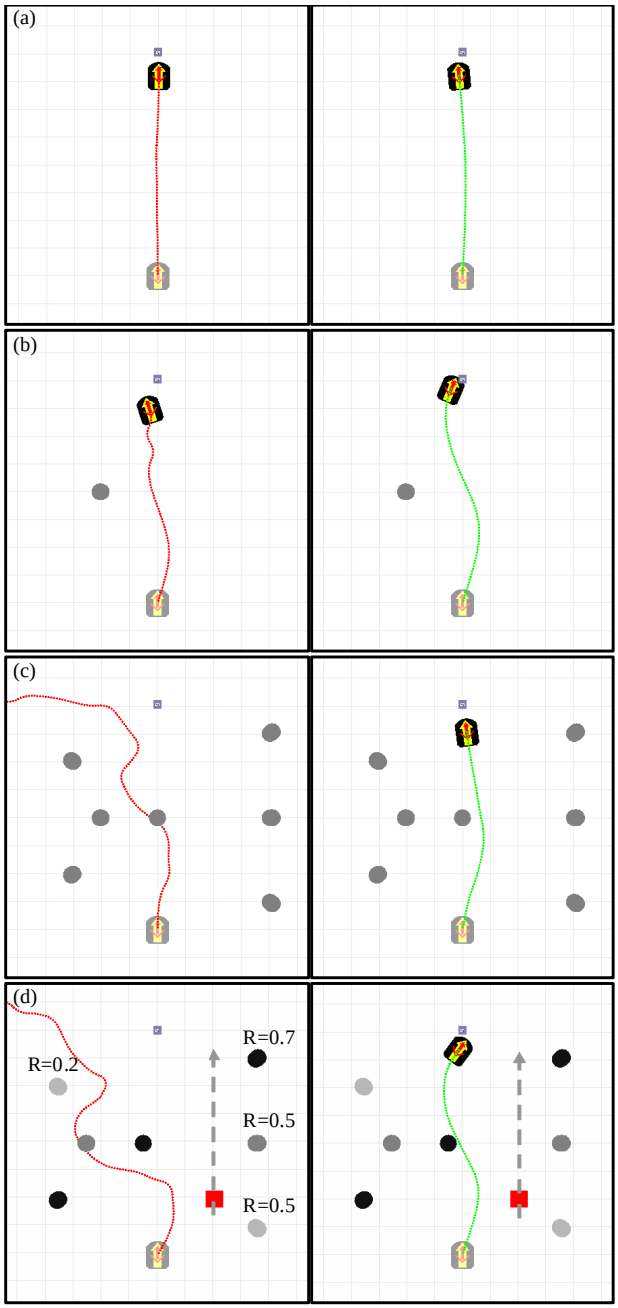

Fig. 11 Simulation results under various conditions (a) empty space (b) space with one obstacle (c) space occupied by randomly positioned obstacles (d) space occupied by randomly positioned obstacles with different scattering rates and one moving obstacle

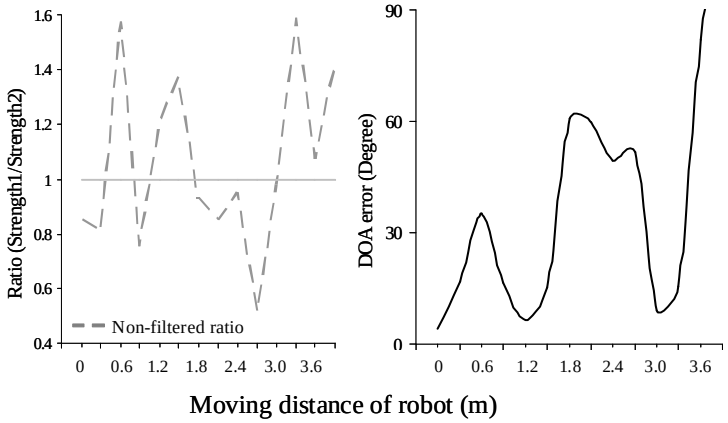

(a) guided by non-filtered ratio

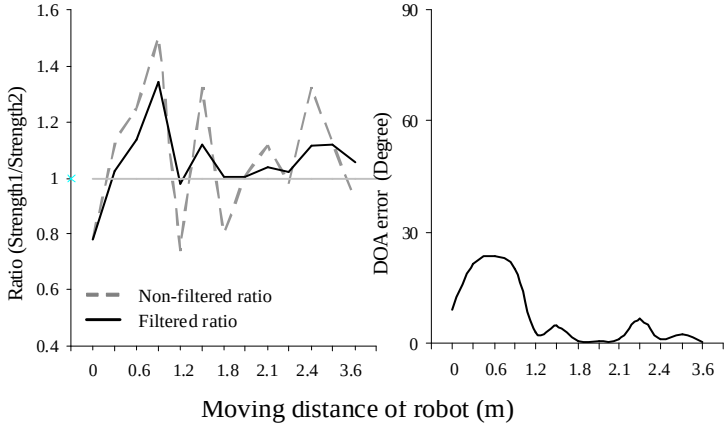

(b) guided by filtered ratio

Fig. 12 Ratio and DOA errors in the case of Fig 11-(c)

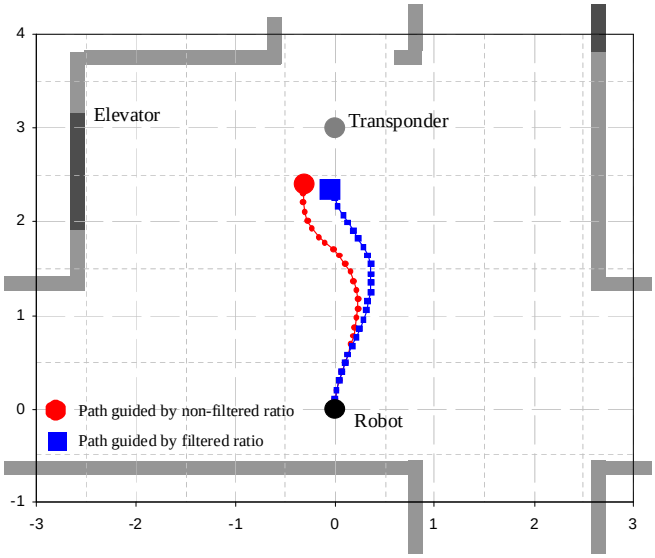

(a) No neighboring obstacle is positioned

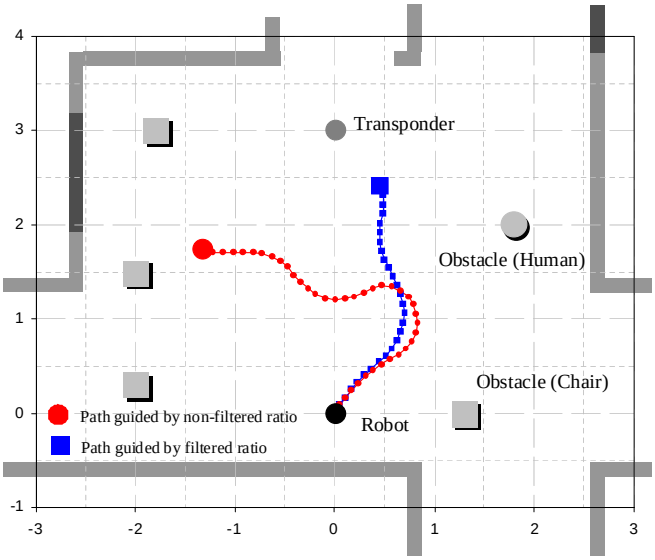

(b) Obstacles positioned in the environment

Fig. 13 Experiment results